ACCOUNTS
of chemical research

Supra- and Nanocrystallinity: Specific Properties Related to Crystal Growth Mechanisms and Nanocrystallinity

M. P. PILENI*

Laboratoire des Matériaux Mesoscopiques et Nanométriques (LM2N), UMR CNRS 7070, Université Pierre et Marie Curie, bât F, BP 52, 4 place Jussieu, 75252 Paris Cedex 05, France

RECEIVED ON FEBRUARY 24, 2012

CONSPECTUS

The natural arrangement of atoms or nanocrystals either in well-defined assemblies or in a disordered fashion induces changes in their physical properties. For example, diamond and graphite show marked differences in their physical properties though both are composed of carbon atoms. Natural colloidal crystals have existed on earth for billions of years. Very interestingly, these colloidal crystals are made of a fixed number of polyhedral magnetite particles uniform in size. Hence, opals formed of assemblies of silicate particles in the micrometer size range exhibit interesting intrinsic optical properties. A colorless opal is composed of disordered particles, but changes in size segregation within the self-ordered silica particles can lead to distinct color changes and patterning.

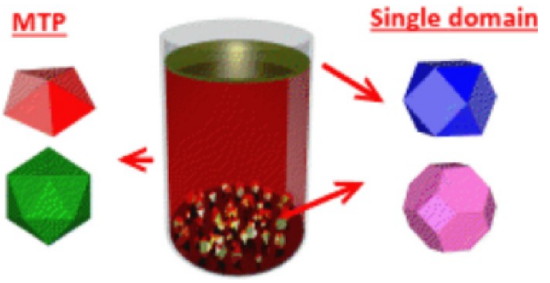

In this Account, we rationalize two simultaneous supracrystal growth processes that occur under saturated conditions, which form both well-defined 3D superlattices at the air–liquid interface and precipitated 3D assemblies with well-defined shapes. The growth processes of these colloidal crystals, called super- or supracrystals, markedly change the mechanical properties of these assemblies and induce the crystallinity segregation of nanocrystals. Therefore, single domain nanocrystals are the primary basis in the formation of these supracrystals, while multiply twinned particles (MTPs) and polycrystals remain dispersed within the colloidal suspension. Nanoindentation measurements show a drop in the Young's moduli for interfacial supracrystals in comparison with the precipitated supracrystals. In addition, the value of the Young's modulus changes markedly with the supracrystal growth mechanism. Using scanning tunneling microscopy/spectroscopy, we successfully imaged very thick supracrystals (from 200 nm up to a few micrometers) with remarkable conductance homogeneity and showed electronic fingerprints of isolated nanocrystals. This discovery of nanocrystal fingerprints within supracrystals could lead to promising applications in nanotechnology.

Introduction

The process of crystal growth leads to the formation of a crystalline solid made of atoms, molecules, or nanoparticles that are typically close packed with fixed positions in space relative to each other. Here we consider crystal growth of atoms and nanocrystals.

Natural colloidal crystals have existed on earth for billions years; some are composed of polyhedral magnetite (Fe_3O_4), crystallites of a few micrometers and uniform in size; those have been identified recently in the Tagish Lake.[1] Very interestingly, these colloidal crystals are made of a fixed number of polyhedral magnetite particles uniform in size. In theory, strong magnetic interactions between nanoparticles are expected to prevent any colloidal crystal formation for particles, in the hundreds of nanometers size range. However, these interactions appear to be rather weak and are attributed to the formation of unusual core–shell structure composed of two different magnetic domains. Other colloidal crystals have been observed in nature. Opals formed of assemblies of silicate particles in the micrometer size range have been shown to exhibit interesting intrinsic optical properties. Silica particles forming either disordered

Published on the Web 09/24/2012 www.pubs.acs.org/accounts
10.1021/ar3000597

or ordered aggregates show marked differences in the optical properties. A colorless opal is made of disordered particles, whereas when the particles are organized, a specific reflectivity can be seen. These physical properties are governed by the particle size and self-assembly type.[2] The changes in the opal color are due to size segregation occurring within the self-ordered silica particles. Those observations open a new research topic with the emergence of a rather large number of new intrinsic properties. Such colloidal crystals are in fact particles in the micrometer scale, self-assembled in 3D superlattices with well-defined crystalline structures as atoms in bulk materials. A rather nice analogy between what is observed in nature and obtained in experimentally manufactured materials can be drawn. Over the last 15 years,[3−12] self-assemblies of 3D superlattices of inorganic (semiconductors, metals, oxides, etc.) nanoparticles have been produced. These nanocrystal assemblies are called supra- or supercrystals. The major difference between the systems discovered in nature and those engineered in the laboratory is related to the size of the nanocrystals involved in both types of assemblies. In nature, the building blocks are almost 2 orders of magnitude larger than those produced experimentally. Furthermore, nature is able to produce supracrystals with a fixed number of particles; that is not yet possible in the laboratory. These supracrystals are soft crystals. Their growth mechanisms are close to those described a long time ago for solid material. Supracrystals exhibit crystalline structures similar to those observed in bulk materials with the formation of face-centered cubic (fcc), hexagonal compact packing (hcp), and body-centered cubic (bcc) crystals. Their growth mechanisms are close to what is already known for solid materials. The heterogeneous supracrystal growth mechanism induces the formation of nanocrystal films deposited on a substrate. Such a growth process involves attractive interactions between nanocrystals that are stronger than those between the substrate and the nanocrystals.[13] This causes rough multilayer films to grow on the substrate and has been assigned as layer-by-layer supracrystals. In such cases, dislocations as well as pavements due to cracks appear on the nanocrystal film. In the homogeneous supracrystal growth process, nucleation comes from seeds existing in solution and aggregates of highly ordered nanocrystals characterized by well-defined shapes are produced. It has unambiguously been observed that these nanocrystals are ordered at the mesoscopic scale (over distances larger than a few micrometers) in not simply an aesthetic arrangement but the formation of novel materials. Specific, unexpected, and remarkable properties have been found when a number of physical properties of 3D disordered aggregates of nanocrystals are compared with those of their fcc supracrystal counterparts, both structures having been prepared from the very same nanocrystal batches.[14−16] The major findings are related to the coherent vibrations of Ag and Co fcc supracrystals, a narrower distribution of interaction energies, and an inhibition of the flipping of the super spins, as well as a slower approach to magnetic saturation compared with Co supracrystals in their disordered form.

Others analogies between nature and engineered materials concerning the crystal growth mechanism and also the ordering of atoms in the final materials can be made. We know that the ordering of atoms in bulk material critically changes the properties of the matter in nature. One of the most striking examples of such effect is the marked change in the physical properties of diamond and graphite, although they are both composed of carbon atoms. At the nanoscale, the influence of the crystalline structure, also called nanocrystallinity, on the chemical and physical properties of nanocrystals remains an open and controversial question.[17] This is mainly due to technical challenges in producing nanocrystals of chosen nanocrystallinity. However, despite the difficulties in synthesizing well-structured nanocrystals, various studies on their physical properties have been carried out over the past few years, one of the most developed research areas nowadays dealing with the influence of the nanocrystallinity on the acoustic vibrational properties of the nanocrystals. The fundamental radial breathing mode ($l = 0$), which can be observed by low-frequency Raman scattering (LFRS), requires nanocrystals with a very low size distribution. A second and somewhat less restrictive approach in terms of size distribution deals with dynamic pump−probe experiments. Built on those two systems, two models were developed from which it is expected that the breathing mode remains mostly unchanged regardless of the nanocrystallinity.[18,19] This was recently confirmed experimentally.[20] However, it is to be noted those results are in opposition with those reported by Tang et al.[21] for 10 nm Ag nanocrystals for which the frequency of the breathing mode was dependent on the nanocrystallinity. The quadrupolar vibrational mode ($l = 2$) of nanocrystals, which can easily be detected through their LFRS spectra, is split in 2-fold degenerate E_g modes and 3-fold degenerate T_{2g} modes for single domain nanocrystals. In contrast, multiply twinned particles (MTPs) and polycrystals exhibit only one band due to light scattering induced by their quadrupolar vibrational modes.[22,23] Some controversies have emerged regarding

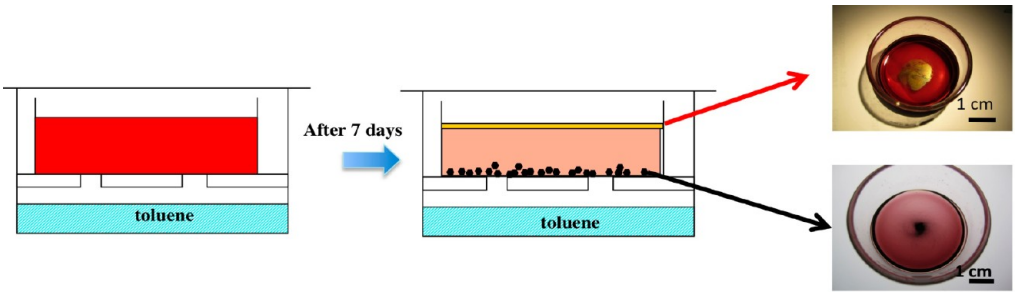

FIGURE 1. Description of the set up with up and down side views of the colloidal solution after 7 days.

the mechanical properties of nanocrystals and the differencies that might originate from their nanocrystallinity. Tang et al.[21] suggested an increase of the Young modulus, deduced from the changes in the fundamental breathing mode for 10 nm Ag nanocrystals. The study of the compressibility of 10 nm Ag and 30 nm Au nanoparticles confirms a significantly higher stiffness than the corresponding bulk phase, such behavior being attributed to the presence of twinned defects.[24] The influence of the nanocrystallinity on the chemical properties of nanocrystals has not been reported, yet. Nevertheless, supersaturation of lattice vacancies caused by the atomic diffusivity (the nano-Kirkendall effect) has been described; the formation of hollow Ag_2Se nanoparticles with single domain 10 nm Ag nanocrystals has been observed, whereas perfect Ag_2Se solid is obtained with MTP nanocrystals.[25] These divergences in the results can be easily explained by the very high difficulty in producing separately either single domain nancrystals or polycrystalline nanoparticles. This clearly shows a need to develop new approaches to select nanocrystallinity.

Here we describe a new method to grow supracrystals that induces both segregation in crystallinity of nanocrystals and specific physical properties: Au nanocrystals dispersed in toluene are kept in supersaturation regime.[26] Simultaneously, flocculation at the air–toluene interface with formation of a film and precipitation of well-defined aggregates take place. The interfacial film and precipitate are both composed of Au nanocrystals ordered in compact fcc structure with similar interparticle distances. Such simultaneous supracrystal growth processes induce nanocrystallinity segregation with supracrystals of single domain nanocrystals.[27] Mechanical properties[28] related to supracrystals differing either by their crystal growth mechanisms or the crystalline structure of the nanoparticles of which they are made have emerged.

Results and Discussion

Two Simultaneous Supracrystal Growth Mechanisms[26,29]. Dodecanethiol-coated Au nanocrystals, having average sizes of 5, 6, 7, and 8 nm (hereby called Au_5, Au_6, Au_7, and Au_8, respectively) and characterized by a very low size distribution (<7%) are dispersed in toluene ([Au] = 10^{-2} M) and kept in a beaker in a saturated toluene atmosphere. The nanocrystals consist of a mixture of single domain nanocrystals, MTPs with decahedral and icosahedral shapes, and polycrystals. These properties will be referred to as nanocrystallinity. After 7 days, flocculation of the nanocrystals occurred at the air–toluene interface resulting in the formation of a bright thin interfacial film (Figure 1). Meanwhile, precipitation of Au nanocrystals is also observed in the vessel. As the aggregation of nanocrystals in the form of either a film or a precipitate progresses, the Au nanocrystal concentration in suspension decreases, as can be seen from a lowering of the color intensity of the suspension.

These results are similar for all Au nanocrystal sizes described herein, unless otherwise stated. The interfacial film was withdrawn using a tungsten ring and deposited on a substrate (HOPG or silicon wafer) and covers large surfaces of the substrate (Figure 2a). For any building block size, high-resolution SEM pictures (Figure 2b) exhibit the formation of a well-ordered Au nanocrystal film with very large uniform orientation areas indicating a long coherence length (several micrometers) in the nanocrystal assembly. Terraces with linear steps of various heights (from one to several nanocrystals thicknesses) induced by screw dislocations are observed. For a given concentration of Au nanocrystal stock solution, the thickness of the formed interfacial film remains unchanged, regardless of the nanocrystal size. SAXRD pattern (inset Figure 2a) shows a fcc lattice except for Au_5 where a mixed fcc/bcc structure is observed. This indexation reveals that a common crystallographic axis ([111]) of the supracrystals is normal to the substrate. The average interparticle distance, δ, calculated from the d_{111} spacing ($\delta = 2.3$ nm), is slightly larger than the length of the dodecanethiol molecule in an all-trans configuration (1.8 nm). This clearly indicates that a layer-by-layer (heterogeneous) growth process occurs at the toluene–air interface behaving as a "substrate".

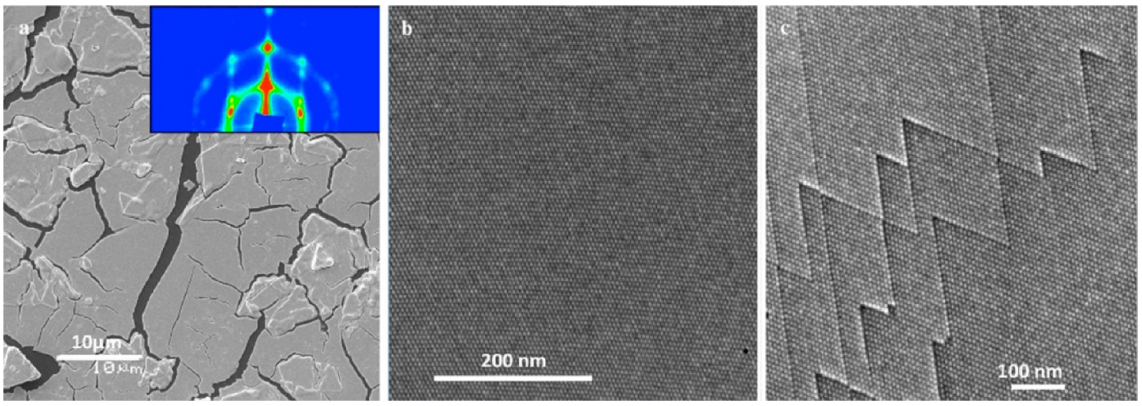

FIGURE 2. (a) SEM image of the interfacial film. Inset: grazing incidence small angle X-ray diffraction of the interfacial film. High resolution SEM images of selected areas on the film showing (b) large domain and with (c) sparse screw dislocations.

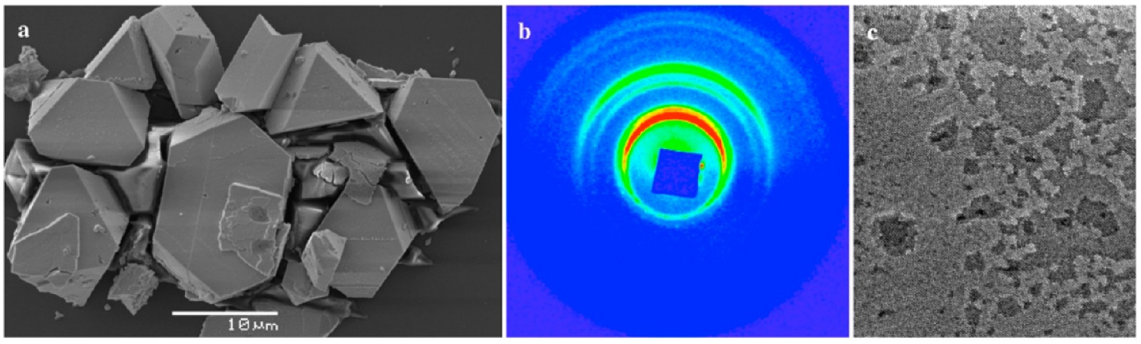

FIGURE 3. (a) SEM image of the Au_5 precipitate, (b) Grazing incidence small angle X-ray diffraction of the precipitate, and (c) high-resolution SEM of a precipitate supracrystal surface.

The precipitate collected at the bottom of the beaker and deposited onto a substrate is composed of individual aggregates of well-defined shapes with an average size ranging between 1 and 10 μm (Figure 3a). Some of the structures appear to be rather flat with well-defined edges whereas others display a 5-fold symmetry shape. The SAXRD pattern (Figure 3b) displaying continuous rings indicates no preferential orientation. Each line of the different profiles is indexed using a fcc structure. It is to be noted that a similar homogeneous nucleation for large Au nanocrystals has been observed in various solvents.[7,12,30] The interparticle distance remains unchanged compared with that obtained with the interfacial film. Note that the size of the precipitated supracrystals is larger for Au_5 nanocrystals than the other assemblies (Au_6 to Au_8).

Note that, for any nanocrystal size, the interfacial and precipitated supracrystals as characterized by interparticle distances, determined from SAXRD patterns, are similar (Table 1).

From these data, it can be inferred that two simultaneous supracrystal growth mechanisms take place at thermodynamic equilibrium with a layer-by-layer (heterogeneous) supracrystal growth at the air−toluene interface and in solution (homogeneous).

Regarding the analogy between what is observed in nature and what is obtained for experimentally manufactured materials in confined media, such as the conditions that are found naturally in some underground pools in central Texas (U.S.A.), aragonite crystals form and float at the air−water interface, mimicking a nearly flat perfect substrate property.[31] Figure 4 clearly show a "quasi"-perfect flat surface produced by interfacial crystal growth processes either in underground pools or in the laboratory. Figure 4a shows the SEM image of bulk aragonite crystal composed of atoms, whereas Figure 4b is an SEM image of interfacial supracrystals made of Au nanocrystals.

Stiffness of Supracrystals Differing by Their Growth Mechanisms[28]. The physical properties of those 3D structures depending on their growth mechanism were investigated by nanoindentation measurements using an AFM tip. Two models (Oliver and Pharr and plate) were used to determine the Young's moduli of the supracrystals. The values deduced from these two models slightly differ, but they are in the same order of magnitude. Furthermore, the

TABLE 1. Nanocrystal Characteristics for Each Supracrystal

		Au_5	Au_6	Au_7	Au_8
mean diameter (nm)		5.2	6.1	7.0	7.8
polydispersity (%)		7	6	6	8
interparticle distance (nm)	interface	2.3 ± 0.4	2.3 ± 0.4	2.1 ± 0.4	2.0 ± 0.3
	precipitate	2.1 ± 0.1	2.4 ± 0.4	2.6 ± 0.4	2.5 ± 0.3

changes in the behavior for interfacial and precipitated supracrystals remain similar. For Au_5 interfacial supracrystals, the Young's moduli, according the two models used, are estimated to be 1.1 and 0.24 GPa, respectively. Conversely, the Young's modulus for Au_5 precipitated supracrystals is estimated to 5 GPa. Hence, the Au_5 supracrystals produced in solution via an homogeneous growth process are characterized by a Young's modulus with a value 5 times larger than those produced at the air−toluene interface by a heterogeneous growth process. Independent sets of experiments were carried out several times on several samples; the observations described above proved to be highly reproducible. Note that the average distance between nanocrystals remains unchanged, regardless of the supracrystal growth process (Table 1). A size segregation process between nanocrystals occurring at the interface and the precipitate can be ruled out since similar size distribution values were recorded from the nanocrystals originating from either the interface or the precipitate.

The origin of the observed discrepancies in the Young's modulus values needs to be addressed. They can arguably be attributed to the origin of the supracrystal growth process. In order to confirm such a hypothesis, the Au_5 precipitated supracrystals were extracted from the bottom of the beaker and dissolved in hexane. An optically clear solution of Au nanocrystals was obtained. Then, a substrate was deposited at the bottom of the cell, and the solvent was allowed to slowly evaporate. As expected from previous experiments,[12] a layer-by-layer supracrystal film was formed. The average Young's moduli corresponding to the layer-by-layer supracrystals, deduced from the two models, are 1.1 and 0.55 GPa. These values are in complete agreement with the data obtained with Au_5 interfacial supracrystals, also grown via a layer-by-layer mechanism (heterogeneous). Hence, the Young's moduli of Au_5 supracrystals produced by evaporation of nanocrystals initially grown in solution (1.1 and 0.55 GPa) are similar to those measured at the air−toluene interface (1.1 GPa and 0.24 GPa). They show a 5-fold decrease compared with the corresponding Au_5 precipitated supracrystals produced by using the same batch of Au_5 nanocrystals. Hence, the average Young's modulus markedly changes with the process involved in the production of

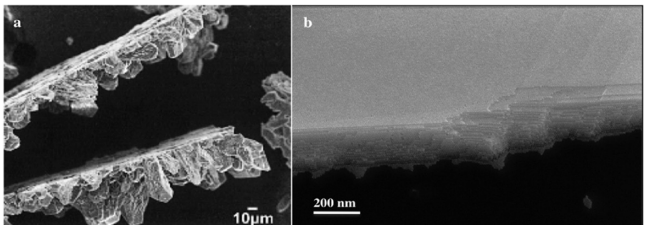

FIGURE 4. (a) SEM image of aragonite crystals produced underground pools (ref 31). (b) Titled SEM image of interfacial supracrystals of 6 nm Au nanocrystals.

supracrystals, indicating that the supracrystal growth mechanism is a key parameter in the stiffness of the final product. Rationalizing those results remains challenging since the average distance between nanocrystals is unchanged for interfacial and precipitated supracrystals. One can argue that some solvent molecules are trapped in the lattice interstices of the interfacial films while these interstitial solvent molecules are absent in the precipitated supracrystals. It should be mentioned that the presence of cracks and dislocations also indicate that solvent molecules are associated with the interfacial supracrystals before they are deposited on the substrate.

Nanocrystallinity Segregation[27]**.** As reported above, it is possible to distinguish monodomain nanocrystals and polycrystals through their acoustic vibrations since a splitting of the quadrupolar modes in 2-fold degenerate E_g modes and 3-fold degenerate T_{2g} modes occurs for single domain nanocrystals. In contrast, only one band is observed in the case of MTPs and polycrystals due to light scattering induced by their quadrupolar vibrational modes.[32] Stokes/anti-Stokes low-frequency Raman scattering (LFRS) spectra were recorded on the Au_5 interfacial (Figure 2a) and precipitated (Figure 3a) supracrystals and those produced by evaporation of the remaining solution (Figure 4d) in equilibrium between the interfacial and precipitated supracrystals (Figure 1). The LFRS spectra of the Au_5 interfacial film (Figure 5a) and precipitated supracrystals (Figure 5c) exhibit two distinct Raman bands peaks in the 135−210 GHz region. Such splitting of quadrupolar modes is unambiguously attributed to single domain nanocrystals. In contrast, a larger band is observed in the spectrum of nanocrystals remaining in suspension (Figure 5b). This multicomponent band is attributed to the mutual contributions of single

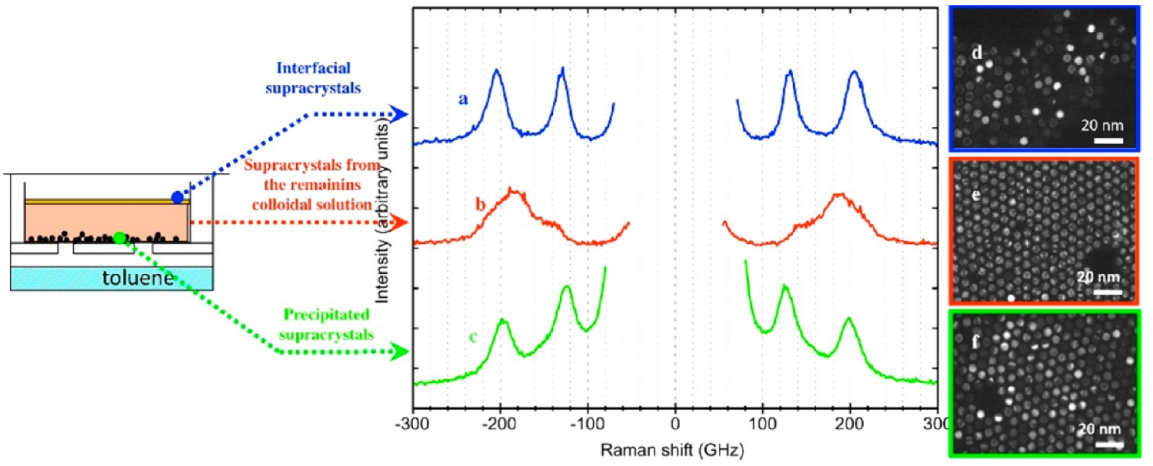

FIGURE 5. Anti-Stokes/Stokes low-frequency Raman spectra (l_{exc}= 561 nm) of interfacial (a) and precipitated (c) supracrystals (blue and green curves, respectively) and supracrystals (b) produced by evaporation of the colloidal solution (red curve) of Au_5 nanocrystals. Conical dark field images of Au_5 nanocrystals (d, e, f) obtained from interfacial (d), precipitated (f), or the remaining colloidal solution in equilibrium with the two supracrystals (e).

domain and polycrystalline nanocrystals. This indicates that supracrystals (interfacial and precipitated) are composed of single domain nanocrystals whereas MTPs and polycrystals remain in solution.

The dark field TEM images obtained on Au_5 interfacial film and precipitated supracrystals after they have been extracted from the vessel and suspended separately in hexane and deposited on a TEM grid confirms this claim. Those results are depicted in Figure 5d,f, respectively; a homogeneous contrast on these pictures indicates that the nanocrystals are single domain. The same experiment was carried out with a drop of the solution in equilibrium with interfacial and precipitated supracrystals, the resulting TEM dark field image is presented in Figure 5e. The inhomogeneous contrast (compared with Figure 5d,f) is attributed to the presence of a mix of nanocrystals having either MTP or polycrystal structure. From LFRS and dark field TEM images, it is concluded that the simultaneous supracrystal growth process at the air–toluene interface and in solution induces the nanocrystallinity selection. This process is obvious for Au_5 nanocrystals. Built on these observations, it can be concluded that Au_5 supracrystals (interfacial and precipitated) are composed of single domain Au_5 nanocrystals whereas those originating from the remaining solution are composed of MTPs and polycrystals. This clearly shows that the simultaneous Au_5 supracrystal growth processes permit the nanocrystallinity selection. When the nanocrystal size is increased, the nanocrystallinity selection is continuously less pronounced and tends to completely disappear in the case of Au_7 and Au_8 nanocrystals.

Transport Properties[33,34]**.** We succeeded in imaging the surface of the Au_7 interfacial and precipitated supracrystals

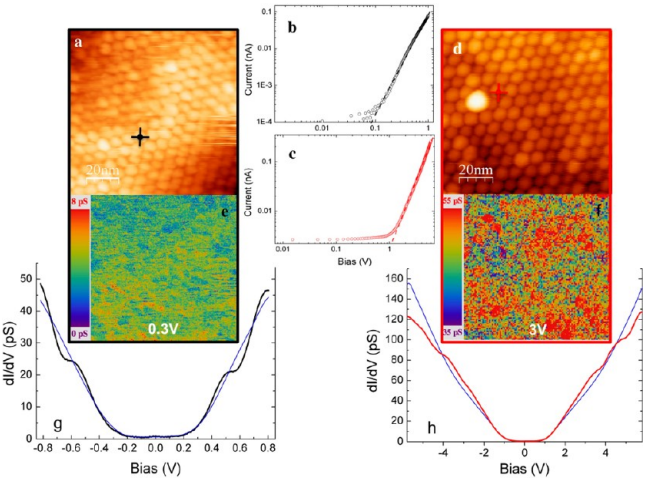

FIGURE 6. STM/STS of interfacial and precipitated supracrystals on HOPG. (a) typical 100 × 100 nm^2 topographic STM image of the interfacial supracrystal with tunnelling current set-point at 130 pA and bias voltage at 2.3 V. (b) log(*I*) vs log(*V*) spectrum taken at the position indicated in panel a (black cross). (c) log(*I*) vs log(*V*) spectrum taken at the position indicated in panel d (red cross). (d) Typical 100 × 100 nm^2 topographic STM image of the precipitated supracrystal with tunnelling current set-point at 200 pA and bias voltage at 5.0 V. (e) Differential conductance map at 0.3 V of the STM image presented in panel a. (f) Differential conductance map at 2 V of the STM image presented in panel 6d. (g) Averaged differential conductance vs *V* curve (blue line) corresponding to STM image presented in panel a to a single nanocrystal of the interfacial supracrystal (black line). (h) Averaged differential conductance vs *V* curve (black line) corresponding to the STM image presented in panel d and to one single nanocrystal of the precipitated supracrystal (red line).

by STM at 5 K. Contrary to what is expected, these thick supracrystals are conductive enough to nanocrystals in hexagonal lattice (Figures 6a,c). The supracrystals are highly stable for all thicknesses (200 nm to 5 mm) during imaging with bias voltages up to 9 V. Such a high voltage suggests

that the potential drop between the STM tip and the first nanocrystal layer of such supracrystals is not equal to the applied voltage but is instead markedly reduced due to the highly resistive nature of the films. In a standard STM experiment with a tip in front of a simple metallic surface, at 9 V, the junction would be in strong field-emission regime, and the field-emitted electrons would certainly severely damage the sample. Here, the nanocrystals are coated with dodecanthiol molecules, which play the role of a dielectric barrier. Then the nanocrystals in the supracrystal act as voltage dividers. Hence the current passes across the supracrystalline network via tunneling effects between nanocrystals. Such process confers a very high resistivity to the supracrystals[35,36] and a large voltage drop across the layers is observed. Then, the voltage drop between the STM tip and the first nanocrystal layer of the supracrystal is much lower than the applied voltage, in particular in the case of the precipitated supracrystals. Of course, the voltage drop through the film increases when the number of nanocrystal layers increases, explaining why imaging of the very thick precipitated supracrystals necessitates higher voltages compared with the thinner supracrystal (interfacial). Local spectroscopic measurements were also carried out in order to gain some insight on the transport mechanism involved. All the experiments were carried out several times. The average conductance curve, $I(V)$, shows a clear power law dependence $I(V) \propto (V - V_T)^{\zeta}$ characteristic of collective Coulomb blockade regime;[37] ζ is independent of the thickness (from 200 nm to few micrometers) and is around 3. The fact that the scaling exponents are comparable for interfacial and precipitated supracrystals seems to indicate that similar transport mechanism takes place for supracrystals having around 40 and 700 nanocrystal layers. This confirms that a key parameter in the transport mechanism is the number of nanocrystal layers as has been demonstrated for 2D lateral transport.[38] Preliminary results indicate that thinner supracrystal films exhibit a ζ factor of 1.3. Nevertheless the threshold voltage, V_T, increases with the supracrystal thickness; therefore the V_T value is larger in the case of precipitated supracrystals compared with interfacial supracrystals. The dI/dV curves measured above a given NC exhibit a slight additional modulation superimposed to the collective $(V - V_T)^{\zeta-1}$ conductance background that mimics the Coulomb staircase structure normally associated with Coulomb blockade by an individual nanocrystal.[39] Apart from this slight Coulomb oscillation, the conductance background is very homogeneous all over the surface as shown at 0.3 V (Figure 6g) and 3 V (Figure 6h) for interfacial and precipitated supracrystals, respectively. This is attributed to the high ordering of nanocrystals in the supracrystals and to the low nanocrystal size distribution. All these results may suggest that nanocrystals within supracrystals are electrically weakly coupled, thus inducing a collective Coulomb gap with only few nanocrystals participating in the conductivity mechanism of thick supracrystals, the others acting as dielectric media. Hence, the similar electronic behavior between these supracrystals (interfacial and precipitate) may indicate identical transport mechanisms. This has to be clarified in future investigations and could be important for future applications.

Conclusions

Similarly to calcite crystallization processes that can occur at the water/air interface, naturally formed in some underground pools,[31] two simultaneous growth processes are shown to produce supracrystals from Au nanocrystal colloidal solution. These growth mechanisms, at the equilibrium, permit production of highly homogeneous supracrystals with very few defects. Two supracrystal mechanisms (heterogeneous and homogeneous) are described. Furthermore unexpected physical properties are observed; for a given Au nanocrystal size, the cooresponding supracrystal mechanical properties markedly depend on the supracrystal growth mechanism. Nanocrystallinity selection with formation of supracrystals of single domain nanocrystals is achieved, while MTPs and polycrystals are naturally discarded and left in suspension. The selective production of a population of single domain nanocrystals and MTPs by soft chemical processes is highly challenging. Here, a new synthetic route is described to this end. Finally, it is shown for the first time that very thick supracrystals can be imaged by STM, and the conductance, highly homogeneous, still keeps the electronic fingerprints of isolated NC. Note that there was similar behavior in electronic transport properties of supracrystals markedly differing by their stiffnesses.

Special thanks are due to my colleagues and students who participated in work presented here: Drs. I. Arfaoui, T. Cren, N. Goubet, H. Portales, N. Schaeffer, C. Yan, and P. Yang. The research leading to these results has received funding from Advanced Grant of the European Research Council under Grant Agreement No. 267129.

BIOGRAPHICAL INFORMATION

Prof. M. P. Pileni (http://www.sri.jussieu.fr/pileni.htm) is a Distinguished Professor at University P&M Curie, UPMC, and Adjunct Professor of chemistry and biochemistry in the school of chemistry and biochemistry at Georgia Tech, Atlanta, U.S.A. She is member

(1999 to present) and chair (2004−2010) of Institut Universitaire de France, IUF. She has published around 400 articles with 15,690 citations, 47.40 average citations per item, and h factor of 65. She received several awards from United States, Japan, the Netherlands, Germany, Spain, Sweden, and France. She is a member of the European Academy of Science, the Royal Swedish Academy of Engineering Sciences, and the Academiae Europeaae. Prof. Pileni's research has been highly interdisciplinary. Her major breakthroughs are as follows: (i) A fundamental understanding of the kinetics and mechanisms in colloidal solutions guided me in the preparation of either nanocrystals with different sizes and shapes or the chemical modification of enzymes. (ii) Formation of thermodynamically stable states of self-assemblies by using either surfactant molecules or inorganic nanocrystals. (iii) Collective optical and magnetic properties due to the nanocrystal arrangements in 1D, 2D, and 3D superlattices. (iv) Physical intrinsic properties related to the crystalline structure of nanomaterials and to nanocrystal ordering in supracrystals (3D). (v) Chemical intrinsic properties due to nanocrystal ordering.

FOOTNOTES

*E-mail: marie-paule.pileni@upmc.fr.
The authors declare no competing financial interest.

REFERENCES

1 Nozawa, J.; Tsukamoto, K.; van Enckevort, W.; Nakamura, T.; Kimura, Y.; Miura, H.; Satoh, H.; Nagashima, K.; Konoto, M. Magnetite 3D Colloidal Crystals Formed in the Early Solar System 4.6 Billion Years Ago. *J. Am. Chem. Soc.* **2011**, *133*, 8782–8785.

2 Sanders, J. V. Color of Precious Opal. *Nature* **1964**, *204*, 1151–1153.

3 Motte, L. F.; Billoudet, F.; Pileni, M. P. Self Assembled Monolayer of Nanosized Particles Differing by Their Sizes. *J. Phys. Chem.* **1995**, *99*, 16425–16429.

4 Murray, C. B.; Kagan, C. R.; Bawendi, M. G. Self-Organization of CdSe Nanocrystallites into Three-Dimensional Quantum Dot Superlattices. *Science* **1995**, *270* (5240), 1335–1338.

5 Whetten, R. L.; Shafigullin, M. N.; Khoury, J. T.; Schaaff, T. G.; Vezmar, I.; Alvarez, M. M.; Wilkinson, A. Crystal Structures of Molecular Gold Nanocrystal Arrays. *Acc. Chem. Res.* **1999**, *32*, 397–406.

6 Korgel, B. A.; Fitzmaurice, D. Small-Angle X-ray-Scattering Study of Silver-Nanocrystal Disorder-Order Phase Transitions. *Phys. Rev. B* **1999**, *59*, 14191–14201.

7 Compton, O. C.; Osterloh, F. E. Evolution of Size and Shape in the Colloidal Crystallization of Gold Nanoparticles. *J. Am. Chem. Soc.* **2007**, *129*, 7793–7798.

8 Prasad, B. L. V.; Sorensen, C. M.; Klabunde, K. J. Gold Nanoparticle Superlattices. *Chem. Soc. Rev.* **2008**, *37*, 1871–1883.

9 Henry, A. I.; Courty, A.; Pileni, M. P.; Albouy, P. A.; Israelachvili, J. Tuning of Solid Phase in Supracrystals Made of Silver Nanocrystals. *Nano Lett.* **2008**, *8*, 2000–2005.

10 Rupich, S. M.; Shevchenko, E. V.; Bodnarchuk, M. I.; Lee, B.; Talapin, D. V. Size-Dependent Multiple Twinning in Nanocrystal Superlattices. *J. Am. Chem. Soc.* **2010**, *132*, 289–296.

11 Courty, A. J.; Richardi, J.; Albouy, P. A.; Pileni, M. P. How to Control the Crystalline Structure of Supracrystals of 5-nm Ag Nanocrystals. *Chem. Mater.* **2011**, *23*, 4186–4192.

12 Goubet, N.; Richardi, J.; Albouy, P. A.; Pileni, M. P. Which Forces Do Control the Supracrystal Nucleation in Organic Media? *Adv. Funct. Mater.* **2011**, *21*, 2693–2704.

13 Motte, L.; Lacaze, E.; Maillard, M.; Pileni, M. P. Self-Assemblies of Silver Sulfide Nanocrystals on Various Substrates. *Langmuir* **2000**, *16*, 3803–3812.

14 Pileni, M. P. Nanocrystal Self-Assemblies: Fabrication and Collective Properties. *J. Phys. Chem. B* **2001**, *105*, 3358–3371.

15 Pileni, M. P. Self-Assembly of Inorganic Nanocrystals: Fabrication and Collective Intrinsic Properties. *Acc. Chem. Res.* **2007**, *40*, 685–693.

16 Pileni, M. P. Supracrystals of Inorganic Nanocrystals: An Open Challenge for New Physical Properties. *Acc. Chem. Res.* **2008**, *41*, 1799–1809.

17 Pileni., M. P. Supra- and Nanocrystallinities: A New Scientific Adventure. *J. Phys.: Condens. Matter* **2011**, *23*, 503102.

18 Saviot, L.; Murray, D. B. Acoustic Vibrations of Anisotropic Nanoparticles. *Phys. Rev. B* **2009**, *79*, No. 214101.

19 Crut, A.; Maioli, P.; Del Fatti, N.; Vallee, F. Anisotropy Effects on the Time-Resolved Spectroscopy of the Acoustic Vibrations of Nanoobjects. *Phys. Chem. Chem. Phys.* **2009**, *11* (28), 5882–5888.

20 Polli, D.; Lisiecki, I.; Portalès, H.; Cerullo, G.; Pileni, M. P. Low Sensitivity of Acoustic Breathing Mode Frequency in Co Nanocrystals upon Change in Nanocrystallinity. *ACS Nano* **2011**, *5*, 5785–5791.

21 Tang, Y.; Ouyang, M. Tailoring Properties and Functionalities of Metal Nanoparticles through Crystallinity Engineering. *Nat. Mater.* **2007**, *6*, 754–759.

22 Portales, H.; Goubet, N.; Saviot, L.; Adichtchev, S.; Murray, D. B.; Mermet, A.; Duval, E.; Pileni, M. P. Probing Atomic Ordering and Multiple Twinning in Metal Nanocrystals through Their Vibrations. *Proc. Natl. Acad. Sci. U.S.A.* **2008**, *105*, 14784–14789.

23 Portales, H.; Goubet, N.; Saviot, L.; Yang, P.; Sirotkin, S.; Duval, E.; Mermet, A.; Pileni, M. P. Crystallinity Dependence of the Plasmon Resonant Raman Scattering by Anisotropic Gold Nanocrystals. *ACS Nano* **2010**, *4*, 3489–3497.

24 Gu, Q. F.; Krauss, G.; Steurer, W.; Gramm, F.; Cervellino, A. Unexpected High Stiffness of Ag and Au Nanoparticles. *Phys. Rev. Lett.* **2008**, *100*, No. 045502.

25 Zhang, Q.; Wang, W.; Goebl, J.; Yin., Y Self-Templated Synthesis of Hollow Nanostructures. *Nano Today* **2009**, *4*, 494–507.

26 Goubet, N.; Portales, H.; Yan, C.; Albouy, P. A.; Pileni, M. P. Simultaneous Growths of Gold Colloidal Crystals. *J. Am. Chem. Soc.* **2012**, *134*, 3714–3719.

27 Portalès, H.; Goubet, N.; Sirotkin, S.; Duval, E.; Mermet, A.; Albouy, P. A.; Pileni, M. P. Crystallinity Segregation upon Selective Self-Assembling of Anisotropic Au Single Nanocrystals in Colloidal Solution. *Nano Lett.* **2012**, in press.

28 Yan, C.; Arfaoui, I.; Goubet, N.; Pileni, M. P. Soft Supracrystal of Au Nanocrystals with Tunable Mechanical Properties. Submitted for publication.

29 Goubet, N.; Richardi, J.; Albouy, P. A.; Pileni, M. P. Simultaneous Interfacial and Precipitated Supracrystals of Au Nanocrystals: Experiments and Simulations. Submitted for publication.

30 Abecassis, B.; Testard, F.; Spalla, O. Gold Nanoparticle Superlattice Crystallization Probed In Situ. *Phys. Rev. Lett.* **2008**, *100*, No. 115504.

31 Tayor, P. M.; Chafetz, H. S. Floating Rafts of Calcite Crystals in Cave Pools, Central Texas, USA: Crystal Habit vs. Saturation State. *J. Sediment. Res.* **2004**, *74*, 328–341.

32 Duval, E. Far-infrared and Raman Vibrational Transitions of a Solid Sphere: Selection Rules. *Phys. Rev. B* **1992**, *46*, 5795–5797.

33 Yang, P.; Arfaoui, I.; Cren, T.; Goubet, N.; Pileni, M. P. Unexpected Electronic Properties of Micrometer-Thick Supracrystals of Au Nanocrystals. *Nano Lett.* **2012**, *12*, 2051–2055.

34 Yang, P.; Arfaoui, I.; Cren, T.; Goubet, N.; Pileni, M. P. Electronic Properties Probed by Scanning Tunneling Spectroscopy: From Isolated Fold Nanocrystals to Well-defined Supracrystals. *Phys. Rev. B* **2012**, *86*, 075409,1−6.

35 Zabet-Khosousi, A.; Dhirani, A. A. Charge Transport in Nanoparticle Assemblies. *Chem. Rev.* **2008**, *108*, 4072–4124.

36 Jeffrey, L. D.; Al-Amin, D. *Nanotechnology* **2008**, *19* (2), No. 025202.

37 Middleton, A. A.; Wingreen, N. S. Collective Transport in Arrays of Small Metallic Dots. *Phys. Rev. Lett.* **1993**, *71*, 3198–3201.

38 Black, C. T.; Murray, C. B.; Sandstrom, R. L.; Sun, S. Spin-Dependent Tunneling in Self-Assembled Cobalt-Nanocrystal Superlattices. *Science* **2000**, *290*, 1131–1134.

39 Bigioni, T. P.; Harrell, L. E.; Cullen, W. G.; Guthrie, D. K.; Whetten, R. L.; First, P. N. Imaging and Tunneling Spectroscopy of Gold Nanocrystals and Nanocrystal Arrays. *Eur. Phys. J. D* **1999**, *6*, 355.